

A New Advanced MRI Biomarker for Remyelinated Lesions in Multiple Sclerosis

Reza Rahmanzadeh, MD, PhD ^{1,2,3} Riccardo Galbusera, MD,^{1,2,3} Po-Jui Lu, PhD,^{1,2,3}
 Erik Bahn, MD,⁴ Matthias Weigel, PhD,^{1,2,3,5} Muhamed Barakovic, PhD,^{1,2,3}
 Jonas Franz, MD,^{4,6,7} Thanh D. Nguyen, PhD,⁸ Pascal Spincemaille, PhD,⁸
 Simona Schiavi, PhD,⁹ Alessandro Daducci, PhD,⁹ Francesco La Rosa, PhD,^{10,11}
 Martina Absinta, MD, PhD ^{12,13} Pascal Sati, PhD,^{14,15} Meritxell Bach Cuadra, PhD,^{10,11}
 Ernst-Wilhelm Radue, MD,^{1,2} David Leppert, MD,^{1,3} Jens Kuhle, MD, PhD ^{1,3}
 Ludwig Kappos, MD,^{1,3} Wolfgang Brück, MD,⁴ Daniel S. Reich, MD, PhD,¹⁴
 Christine Stadelmann, MD ⁴ Yi Wang, MD,⁸ and Cristina Granziera, MD, PhD ^{1,2,3}

Objectives: Neuropathological studies have shown that multiple sclerosis (MS) lesions are heterogeneous in terms of myelin/axon damage and repair as well as iron content. However, it remains a challenge to identify specific chronic lesion types, especially remyelinated lesions, in vivo in patients with MS.

Methods: We performed 3 studies: (1) a cross-sectional study in a prospective cohort of 115 patients with MS and 76 healthy controls, who underwent 3 T magnetic resonance imaging (MRI) for quantitative susceptibility mapping (QSM), myelin water fraction (MWF), and neurite density index (NDI) maps. White matter (WM) lesions in QSM were classified into 5 QSM lesion types (iso-intense, hypo-intense, hyperintense, lesions with hypo-intense rims, and lesions with paramagnetic rim lesions [PRLs]); (2) a longitudinal study of 40 patients with MS to study the evolution of lesions over 2 years; (3) a postmortem histopathology-QSM validation study in 3 brains of patients with MS to assess the accuracy of QSM classification to identify neuropathological lesion types in 63 WM lesions.

Results: At baseline, hypo- and isointense lesions showed higher mean MWF and NDI values compared to other QSM lesion types ($p < 0.0001$). Further, at 2-year follow-up, hypo-/iso-intense lesions showed an increase in MWF. Postmortem analyses revealed that QSM highly accurately identifies (1) fully remyelinated areas as hypo-/iso-intense (sensitivity = 88.89% and specificity = 100%), (2) chronic inactive lesions as hyperintense (sensitivity = 71.43% and specificity = 92.00%), and (3) chronic active/smoldering lesions as PRLs (sensitivity = 92.86% and specificity = 86.36%).

Interpretation: These results provide the first evidence that it is possible to distinguish chronic MS lesions in a clinical setting, hereby supporting with new biomarkers to develop and assess remyelinating treatments.

ANN NEUROL 2022;92:486–502

View this article online at [wileyonlinelibrary.com](https://onlinelibrary.wiley.com/doi/10.1002/ana.26441). DOI: 10.1002/ana.26441

Received Dec 14, 2021, and in revised form Jun 12, 2022. Accepted for publication Jun 14, 2022.

Address correspondence to Dr Granziera, Translational Imaging in Neurology (THiNK) Basel, Department of Biomedical Engineering, University of Basel Gewerbestrasse 14, 4123 Allschwil, Switzerland. E-mail: cristina.granziera@usb.ch

[Correction added on July 28, 2022, after first online publication: Reza Rahmanzadeh's degree was updated.]

From the ¹Neurology Clinic and Policlinic, Departments of Medicine, Clinical Research and Biomedical Engineering, University Hospital Basel and University of Basel, Basel, Switzerland; ²Translational Imaging in Neurology (THiNK) Basel, Department of Biomedical Engineering, University Hospital Basel and University of Basel, Basel, Switzerland; ³Research Center for Clinical Neuroimmunology and Neuroscience Basel (RC2NB), University Hospital Basel and University of Basel, Basel, Switzerland; ⁴Institute of Neuropathology, University Medical Center, Göttingen, Germany; ⁵Division of Radiological Physics, Department of Radiology, University Hospital Basel, Basel, Switzerland; ⁶Max Planck Institute for Experimental Medicine, Göttingen, Germany; ⁷Campus Institute for Dynamics of Biological Networks, University of Göttingen, Göttingen, Germany; ⁸Department of Radiology, Weill Cornell Medical College, New York, NY; ⁹Department of Computer Science, University of Verona, Verona, Italy; ¹⁰Signal Processing Laboratory (LTS5), Ecole Polytechnique Fédérale de Lausanne (EPFL), Lausanne, Switzerland; ¹¹Medical Image Analysis Laboratory (MIAL), Center for Biomedical Imaging (CIBM), Lausanne, Switzerland; ¹²Department of Neurology, Johns Hopkins University School of Medicine, Baltimore, MD; ¹³Institute of Experimental Neurology, Division of Neuroscience, Vita-Salute San Raffaele University and Hospital, Milan, Italy; ¹⁴Translational Neuroradiology Section, National Institute of Neurological Disorders and Stroke, Bethesda, MD; and ¹⁵Department of Neurology, Cedars-Sinai Medical Center, Los Angeles, CA

486 © 2022 The Authors. *Annals of Neurology* published by Wiley Periodicals LLC on behalf of American Neurological Association.

This is an open access article under the terms of the [Creative Commons Attribution-NonCommercial-NoDerivs](https://creativecommons.org/licenses/by-nc-nd/4.0/) License, which permits use and distribution in any medium, provided the original work is properly cited, the use is non-commercial and no modifications or adaptations are made.

Quantitative susceptibility mapping (QSM) quantifies the spatial distribution of magnetic susceptibility within biological tissues¹ and provides a measure that is sensitive to both iron accumulation and myelin content in the brain.² QSM has been used to identify white matter (WM) lesions with a rim of iron-laden macrophages/activated microglia in patients with multiple sclerosis (MS; paramagnetic rim lesions [PRLs]), which histopathologically correspond to chronic active and smoldering lesions.^{3–6} In addition, QSM has also been applied to assess the longitudinal evolution of acute MS lesions over time.⁷ Nevertheless, QSM has not previously been exploited for the classification of MS lesion type heterogeneity in neuropathological studies.

Patients with MS exhibit a variety of lesion types which are characterized by a variable extent of myelin/axon damage and repair and iron content.⁸ MS lesions undergo multiple waves of de- and remyelination, which lead to the final lesion phenotype of demyelinated, partly remyelinated, or fully remyelinated (shadow plaques).⁹ Lesion location (ie, periventricular vs juxtacortical),¹⁰ age (ie, acute vs chronic lesions),¹¹ cellular composition (ie, presence of oligodendrocytes and macrophages/activated microglia),¹² and clinical disease course (ie, relapsing-remitting MS [RRMS] vs progressive MS [PMS])^{10,13} likely contribute to the heterogeneity of remyelination activity.

Axonal damage in MS lesions is largely heterogeneous as well. Acute axonal transection occurs more commonly in active demyelinating lesions, whereas inactive MS lesions show delayed degeneration of long-term demyelinated axons,¹⁴ potentially owing to excitotoxic mechanisms and ongoing innate inflammation.¹⁵ In chronic active and smoldering lesions, extensive axonal damage occurs mostly at the lesion border.⁸

Iron content is likewise extremely diverse across lesion types. Many, but not all, active MS lesions harbor iron-laden macrophages.¹⁶ Shadow plaques contain higher amounts of iron compared to smoldering or inactive MS lesions.¹⁷ Furthermore, chronic active lesions are also characterized by an iron-laden rim of macrophages/activated microglia.³

Currently, MS lesion types can be differentiated neuropathologically,⁹ but the distinction of chronic MS lesion types in vivo (ie, remyelinated vs chronic active/smoldering vs chronic inactive) remains challenging. For this study, we applied a multi-contrast quantitative magnetic resonance imaging (MRI) approach, including QSM, myelin water imaging (MWI), and diffusion MRI, to disentangle lesion phenotypes in vivo in patients with MS.

MWI^{18,19} and biophysical models applied to multi-shell diffusion MRI²⁰ offer more specific surrogate measures of myelin and axon content than other advanced MRI

techniques. MWI quantifies the water between myelin layers by distinguishing multiple water compartments in T2 relaxometry data. Moreover, this measure (eg, myelin water fraction [MWF]) has been validated postmortem.^{21,22}

Multicompartment microscopic diffusion imaging (MCMDI), a technique that quantitates the neurite density index (NDI) of the intra-neurite compartment and the extra-neurite compartments in the brain, has also been applied to patients with MS.^{23,24} The advantage of MCMDI over diffusion tensor imaging (DTI) is that MCMDI does not assume a Gaussian distribution of the diffusion process and hence models non-Gaussian diffusion in biological tissue, providing more specific measures of tissue microstructure.^{25,26}

To distinguish chronic MS lesion types in vivo, we classified MS lesions according to their visual appearance in the QSM maps and studied myelin and axonal content among QSM lesion types using MWF and NDI, both cross-sectionally and longitudinally. Further, we performed a combined histopathology/QSM evaluation in 3 postmortem brains of patients with MS to assess the histopathological correlates of the in vivo QSM classification of MS lesions.

Materials and Methods

In Vivo Cross-Sectional and Longitudinal Studies

Participants. We enrolled 115 patients with MS (76 with RRMS and 39 with PMS) and 76 healthy controls (HCs), and the demographic and clinical characteristics are reported in Table 1.

Inclusion criteria were: (1) MS diagnosis according to McDonald criteria from 2017,²⁷ and diagnosis of active RRMS or inactive PMS, as defined by Lublin et al²⁸; (2) absence of any concomitant psychiatric or neurological disease (excluding headache); and (3) absence of contraindication to MRI. All subjects (patients with MS and HCs) benefitted of a quantitative MRI protocol; qMRI maps were reconstructed as outlined in the section “MR acquisition.”

All patients enrolled in this study also underwent a conventional MRI (cMRI) during the 3 months before the study. All gadolinium (Gd) enhancing lesions in cMRI were excluded from the following analyses. Eleven patients were excluded because of motion artifacts in their QSM images.

All patients had a baseline MRI and 40 patients also had an MRI at follow-up with the same protocol (Fig 1).

The study was approved by the ethics review committee of the University Hospital Basel (institutional review board [IRB] of Northwest Switzerland) and all participants gave written consent prior to the study.

Table 1. Clinical Characteristics of Patients and Healthy Subjects

	Cohort type	Patient with MS	Healthy subjects
Sex, n (male/female)	Cross-sectional	115 (48/67)	76 (31/45)
	Longitudinal	49 (13/27)	-
	Postmortem	3 (2/1)	-
Age, yr, mean \pm SD	Cross-sectional	46 \pm 14	35 \pm 13
	Longitudinal	43 \pm 14	-
	Postmortem	58 \pm 5	-
EDSS score, median (range)	Cross-sectional	3.14 (0–8)	-
	Longitudinal	2.5 (1–7)	-
	Postmortem	4 (2.5–8)	-
Disease course (RRMS/PMS)	Cross-sectional	76/39	-
	Longitudinal	32/8	-
	Postmortem	0/3	-
Disease duration, yr, mean \pm SD	Cross-sectional	9.2 (10.41)	-
	Longitudinal	8.93 (10.09)	-
	Postmortem	16 (7.54)	-
Disease-modifying therapy (n)	Cross-sectional	Untreated (13) Interferon-beta (1) Glatiramer acetate (1) Dimethyl fumarate (15) Fingolimod (9) Natalizumab (4) Rituximab (13) Ocrelizumab (55) Siponimod (2) Teriflunomide (2)	-
	Longitudinal	Untreated (3) Dimethyl fumarate (9) Fingolimod (1) Natalizumab (2) Rituximab (3) Ocrelizumab (22)	-

EDSS = Expanded Disability Status Scale; MS = multiple sclerosis; PMS = progressive multiple sclerosis; RRMS = relapsing-remitting multiple sclerosis.

MR Acquisition. MRI was performed on a 3 T whole-body MR system (Prisma, Siemens Healthcare, Erlangen, Germany) using a 64-channel phased-array head and neck coil. The MRI protocols included: (1) 3D fluid-attenuated inversion recovery (FLAIR) (TR/TE/TI = 5,000/386/1,800 ms) with 1 mm³ isotropic spatial resolution; (2) Fast acquisition with spiral trajectory and adiabatic T2prep (FAST-T2; spiral TR/TE = 7.5/0.5 ms, 6 T2prep times = 0 (T2prep turned

off), 7.5, 17.5, 67.5, 147.5, and 307.5 ms, voxel size = 1.25 \times 1.25 \times 5 mm,³ scan time = 4.5 minutes, as described in (Nguyen et al¹⁹); (3) multi-shell diffusion (TR/TE/ δ / Δ /resolution = 4.5 seconds / 75 ms / 19 ms / 36 ms / 1.8 mm³ isotropic with b-values 0 / 700 / 1,000 / 2,000 / 3,000 s/mm² with 12/6/20/45/66 measurements, respectively, per shell, and a diffusion acquisition with 12 measurements of b-value 0 s/mm² with reversed phase

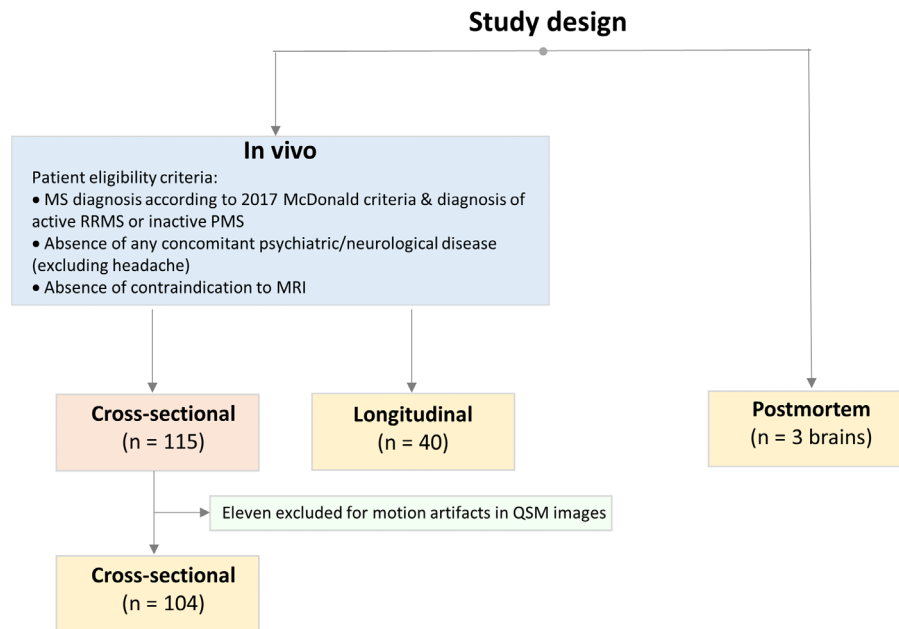


Figure 1: Design of the in vivo and postmortem parts of the study. MS = multiple sclerosis; PMS = progressive multiple sclerosis; QSM = quantitative susceptibility mapping; RRMS = relapsing-remitting multiple sclerosis. [Color figure can be viewed at www.annalsofneurology.org]

encoding as well as (4) 3D segmented echo planar imaging (EPI) with submillimeter isotropic resolution (TR/TE/resolution = 64 ms/35 ms/ $0.67 \times 0.67 \times 0.67 \text{ mm}^3$).

MWF maps were reconstructed using a spatially constrained nonlinear fitting applied to FAST-T2 data.²⁹ In FAST-T2, both the amplitude and phase of adiabatic pulses are modulated under the adiabatic principle,³⁰ which reduces B0/B inhomogeneities effects.

Besides, to reduce potential noise associated with voxel-wise fitting, we incorporated a spatially local smoothness constraint as proposed in Kumar et al.³¹ As explained in Nguyen et al,¹⁹ the regularization parameter was determined by calculating MWF maps for different regularization values in a healthy subject and selecting the one that provided an MWF map with the best visual quality. This optimized value was then fixed for all the subjects enrolled in this study. This approach was shown to produce MWF values in the brain that are comparable with those obtained using a multi-echo spin-echo sequence, which has been validated against histological myelin measurements.³² We have chosen this approach to quantify myelin water, among many available,² because of its robustness against static field (B0) and RF field (B1) inhomogeneities as compared with the traditional hard pulse design, especially at high B0 field strengths.^{19,33,34} Moreover, we opted for this approach because we wanted to avoid spurious susceptibility sensitivity, which had been previously reported for other myelin water imaging acquisition methods³⁴: FAST-T2 samples the T2 signal decay curve starting at 0.5 ms,

rendering it relatively insensitive to the T2-shortening effect of tissue iron.

Diffusion images were denoised and corrected for motion and eddy-currents.³⁵ The MCMDI diffusion model²³ was used, which is a state-of-the-art model that integrates the spherical mean technique to handle orientation dispersion and fiber crossing populations, allowing more accurate estimations in whole-brain voxels. From this model we estimated the NDI, which corresponds putatively to the intra-axonal volume fraction.

The QSM is a field-to-source inversion method to map the local susceptibility sources in the tissue from the shift in the magnetic field created by these sources, which can be measured from gradient echo data. In this study, the QSMs were reconstructed from 3D EPI data by unwrapping phase with the path finding and the signal to noise ratio (SNR) as the image-quality guidance in the region growth method, removing the background field through the Projection onto Dipole Fields algorithm, and using the morphology-enabled dipole inversion algorithm to compute the susceptibility from the local field (MEDI reconstruction), as in Liu et al.³⁶ It has been shown that EPI-QSM provides similar mean susceptibility values compared with standard multi-echo GRE-QSM.^{37,38}

Lesion Identification and Segmentation

Segmentation of WM lesions (WMLs) was performed automatically by using a deep-learning-based method applied to FLAIR and MP2RAGE images.³⁹ Afterward, manual correction of automatic WML was performed as a consensus between 2 experienced

readers (authors R.R. and C.G.). To avoid partial-volume effects due to the different spatial resolution of the applied quantitative maps, we analyzed lesions larger than 10 mm³ in volume.

QSM lesion types were classified as follows: first (1) a map of MS lesions was obtained through automatic detection and segmentation, as detailed above; and then (2) the FLAIR lesion map was registered to the QSM map using a boundary-based registration from the FMRIB software library (FSL)⁴⁰ so that MS lesions could then be identified in the QSM map; afterward, (3) MS lesions were classified according to their appearance on QSM at intensity range ± 200 parts per billion (ppb): (1) iso-intense (ie, lesions that showed no intensity difference in QSM maps compared to the surrounding tissue); (2) hypo-intense lesions; (3) hyperintense lesions; (4) lesions with the hypo-intense rim relative to the lesion center; (5) paramagnetic rim lesions PRL (lesions with hyperintense rim in QSM maps; Fig 2). As shown in a recent

study,⁴¹ MS lesions in QSM often show areas of punctuate hyperintensities, which most likely correspond to vessels containing deoxygenated hemoglobin. In our cohort, these punctate hyperintensities were frequently observed but not considered as a factor influencing the lesion classification. Yet, we cannot exclude that those punctate areas might have contributed to the hyperintensity observed in small sized lesions.

To identify dominantly myelin-damaged and dominantly axon-damaged WM lesions (ie, lesions with a larger percentage change in MWF and NDI, respectively), we calculated the proportion of myelin and axonal damage in WMLs relative to the respective values in the contralateral hemisphere (%MWF and %NDI reduction) as follows⁴²:

$$\left(\frac{[\text{mean MWF or NDI in the mirror region of interest \{ROI\} in the contralateral hemisphere}] - [\text{mean MWF or NDI in lesion}]}{\text{the value in the mirror ROI in the contralateral hemisphere}} \right) \times 100$$

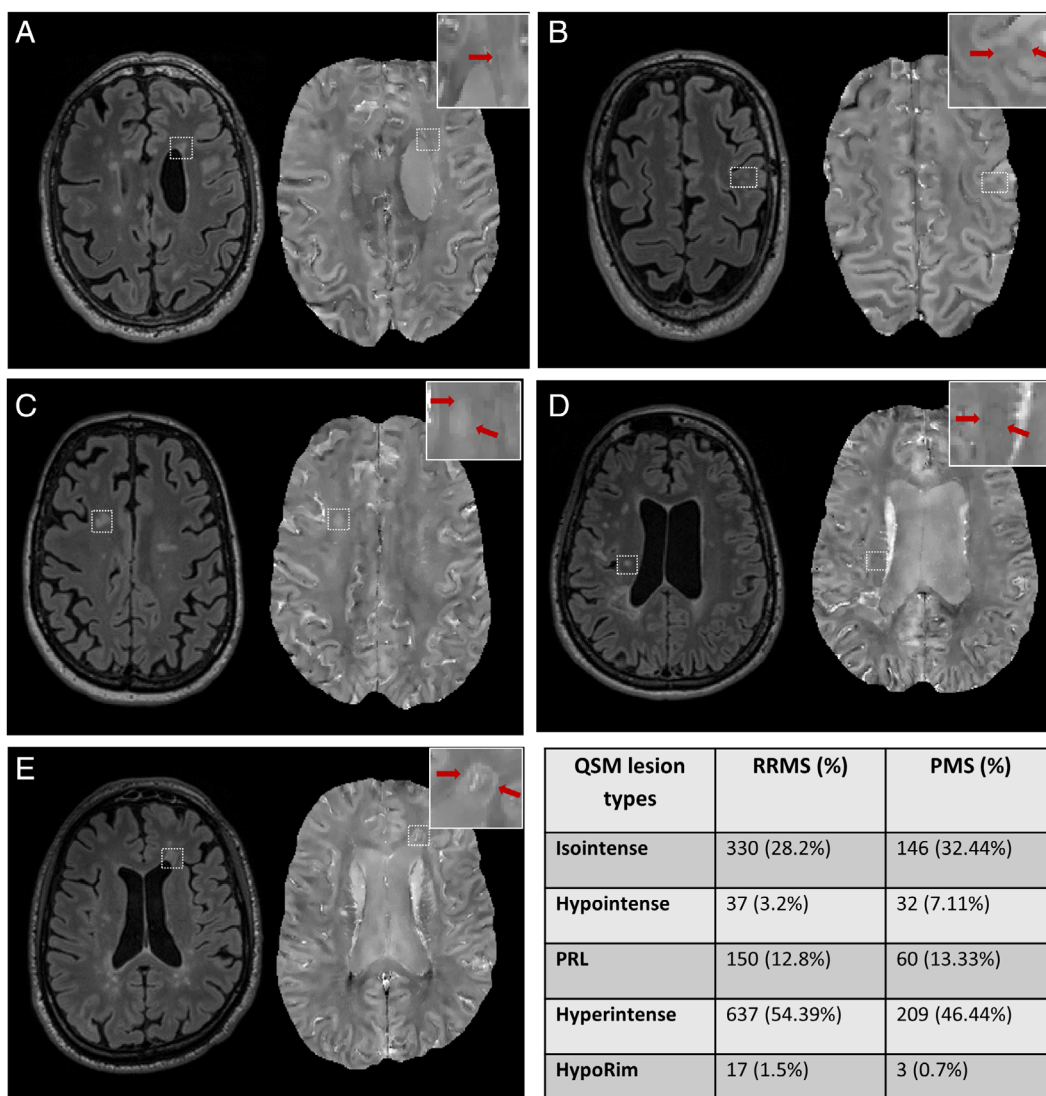


Figure 2: QSM lesion types and their distribution in patients with MS. (A–E) Exemplary QSM lesion types (A = iso-intense, B = hypo-intense, C = hyperintense, D = hypo-rim, E = PRL). Table in Figure 2: distribution of the different QSM lesion types (%) in patients with RRMS and PMS. PMS = progressive multiple sclerosis; QSM = quantitative susceptibility mapping; RRMS = relapsing-remitting multiple sclerosis. [Color figure can be viewed at www.annalsofneurology.org]

For this purpose, all lesions exhibiting contralateral NA mirror areas were selected in the lesion masks. In total, 85 lesions out of 2,852 WMLs were selected and the mirror ROIs were then manually contoured.

Brain WM Segmentation

Using FreeSurfer (version 6.0, surfer.nmr.mgh.harvard.edu),⁴³ the brain was segmented into whole WM, cortex, deep gray matter structures, and ventricles. The normal-appearing white matter (NAWM) mask was produced by subtracting the WM lesion mask from the WM mask.

An in-house algorithm was used to automatically identify a 2-voxel layer of NAWM surrounding the lesions on FLAIR; herein after denoted as peri-plaque WM (PPWM). The relative susceptibility for individual WMLs was calculated as follows: $\text{Susceptibility}_{\text{lesion}} - \text{Susceptibility}_{\text{PPWM}}$.

We further parcellated the WM region into 3 areas exhibiting different anatomic characteristics and proximity to the cerebrospinal fluid/cortex, such as the periventricular area, the juxtacortical area, and the deep WM (PV, JC, and DW, respectively). This allowed us to study the regional distribution of the different QSM lesion subtypes.

All values, including intra-lesional, PP tissue and homogeneous non-lesional NA tissue, were automatically extracted both in lesion-wise and average patient-wise manners.

Clustering of Iso-/Hypo-Intense Lesions vs PRLs

To confirm that the qualitative appearance of QSM lesion types represents lesions with different MWF, NDI, and susceptibility, we applied a Gaussian Mixture Model (GMM) to the lesion groups exhibiting the highest and lowest MWF/NDI/susceptibility mean content. We chose GMM (a method that applies the expectation–maximization algorithm for fitting mixture-of-Gaussian models) instead of the commonly used K-mean algorithm for clustering, because GMM considers also the variance in data to identify clusters whereas K-mean focuses on the data mean to update the centroids.

Finally, we calculated the percentages of QSM lesion types (ie, iso-/hypo-intense lesions vs PRLs) falling into 2 distinct clusters that were identified.

Longitudinal Analysis

In 40 patients, a follow-up MRI was performed after 2 years from baseline. The automatic WM lesion segmentation and manual correction were performed as explained for baseline MRIs ($n = 325$ lesions).

WM lesions were then classified in the follow-up QSM, as described above. Eighteen of 325 lesions (5.53%) exhibited iso- and hypo-intensity in QSM and had a corresponding lesion with a distinct QSM lesion type at baseline.

Statistical Analysis

Statistical analysis was performed using GraphPad Prism version 8.0.0 for Windows, GraphPad Software, San Diego, California, USA.

A Kolmogorov–Smirnov’s test was used to assess the normality of data. Paired t test, nonparametric Mann–Whitney test, and Kruskal–Wallis test with Dunn’s test for multiple comparisons correction were used for the paired 2-group analyses, unpaired 2-group analyses, and the more-than-3 groups analyses, respectively. Spearman correlations were used to assess whether a correlation exists between (1) patient-wise average absolute susceptibility in WML/NAWM or lesion-wise relative susceptibility in WML and (2) disease duration in patients with MS.

Postmortem Imaging and Histopathology

Postmortem MS brains from 3 patients with MS (MS clinical type and age [years]: secondary progressive = 59; secondary progressive = 65; and primary progressive = 66) were imaged on a 3 T hole-body MR system (Prisma^{Fit}, Siemens Healthcare, Erlangen, Germany) using a 20-channel head and neck coil and a dome-shaped brain container filled with per-fluoropolyether. The brains were fixed directly in 4% neutral buffered formaldehyde solution (formalin) within 24 hours after death and for about 4 to 6 months before MRI. Postmortem QSM images were reconstructed using 3D-EPI (330 μm isotropic, TR = 65 ms, TE = 35 ms, and ETL = 13, bandwidth 394 Hz/pixel). We then designed and 3D-printed an individualized cutting box for each brain, as reported previously.⁴⁴ Additional manual registration between the digitized brain slab surfaces and the corresponding MRI slices was performed to further refine the match between histopathological and MRI images. The ROIs including MS lesions were identified and manually segmented on 3D-EPI and FLAIR images using ITK-SNAP version 3.6.0.⁴⁵ As to postmortem 3D EPI and the relative QSM reconstruction, the sequence parameters applied and the contrast window for visual assessments ($-200 + 200$ ppm) were similar to the one used in vivo.

Histopathological Analysis

Three postmortem brains were provided by the MS Brain Bank of the German Competence Network Multiple Sclerosis (KKNMS).

Tissue blocks were embedded in paraffin and 4 μm -slices were stained for myelin (Luxol Fast Blue/Periodic-Acid Schiff [LFB/PAS]), for iron (DAB-enhanced Turnbull staining), as well as using hematoxylin and eosin (H&E) stain.⁹

For immunohistochemistry (IHC), the following primary antibodies were applied: anti-myelin basic protein (MBP; for myelin), anti-CR3/43 (for MHCII-expressing macrophages/activated microglia) IHC, Turnbull’s blue (TBB; for iron) staining, and anti-breast carcinoma-amplified sequence 1 (BCAS1) IHC (for myelin and

actively myelinating oligodendrocytes). Immunohistochemical staining was performed using an avidin–biotin technique. After incubation with the primary antibody (applied at the dilutions indicated by the supplier and incubated overnight at 4°C), antibody binding was visualized using biotinylated secondary antibodies, peroxidase-conjugated avidin and DAB (Sigma-Aldrich). Double-labeling IHC was performed combining DAB and Fast Blue using an alkaline phosphatase-conjugated secondary antibody (Dako, 1:50). Hematoxylin was used as the nuclear counterstain.

After histology/IHC, the sections were scanned automatically by a computer-directed microscope stage (Olympus VS120 Soft Imaging Solutions) under $\times 20$ magnification for further investigations. Digital processing of whole slide images was performed using an open microscopy OMERO server (version 5.6.3).⁴⁶

Remyelination was in LFB/PAS staining and MBP and/or BCAS1 IHC by subtle myelin pallor when compared to the surrounding NAWM, and absence of macrophages with early myelin degradation products. Remyelinated lesions were defined as areas with extensive remyelination covering at least 60% of the lesion surface.¹⁰

Lesion Segmentation and QSM Lesion Classification

WM lesions were manually segmented in 3D EPI images and 3D FLAIR images (authors R.R. and R.G.).

The classification of WM lesions ($n = 63$) in post-mortem QSM (at intensity range ± 200) was performed by an experienced rater (author R.R.) without prior information about neuropathological lesion types, and the sensitivity and specificity of QSM classification to detect remyelinated lesions, chronic inactive, and chronic active MS lesions were reported.

QSM-Histopathology Correlation

A double-blinded analysis was performed to correlate the classification of 63 WM lesions in postmortem QSM images with their respective histopathological types. Reza Rahmanzadeh classified lesions in QSM without any knowledge about histopathological findings, whereas Erik Bahn and Christine Stadelmann classified lesions histopathological without being aware of the QSM-based classification.

Statistical Analysis

We used GraphPad Prism version 8.0.0 for Windows, GraphPad Software, San Diego, California, to assess the sensitivity and specificity of the QSM-classification to specific histopathological lesion groups.

Data Availability

The data that support the findings of this study are available upon reasonable request.

Results

In Vivo Cross-Sectional and Longitudinal Study

Classification of WMLs in Patients With MS on QSM

Maps. The WMLs ($n = 1,621$) showed distinct characteristics within QSM maps and were classified as iso-intense lesions ($n = 476$, 29.4%), hypo-intense lesions ($n = 69$, 4.26%), hyperintense lesions ($n = 846$, 52.2%), lesions with hypo-intense rims (hypo-rim; $n = 20$, 1.23%), and PRLs ($n = 210$, 13%; see Fig 2).

A total of 1,231 lesions were not included in this classification due to (1) the presence of a large vessel traversing the lesion area (75.62%, those were usually small

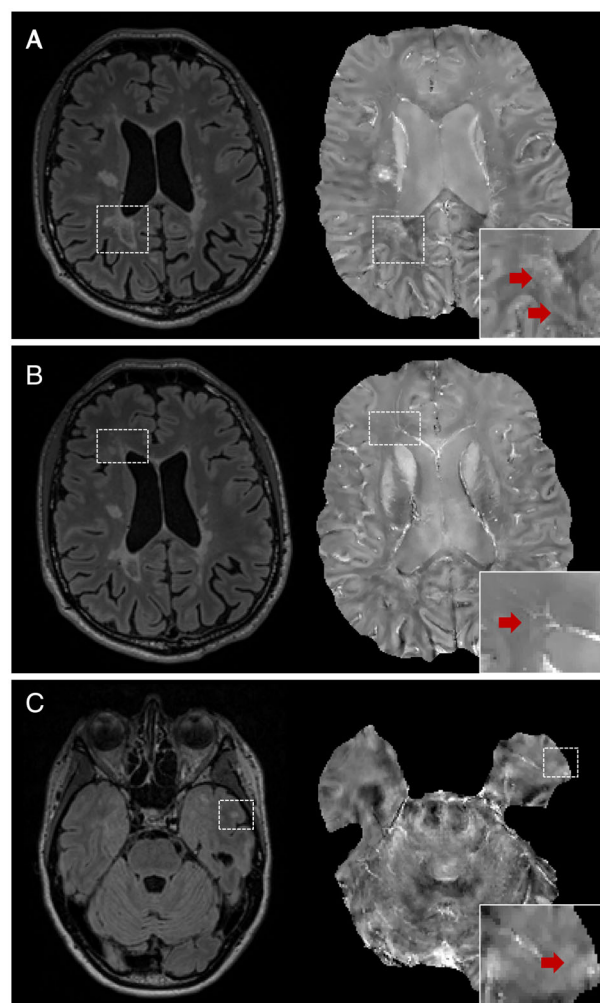


Figure 3: Lesions excluded from the QSM classification. (A) Confluent lesions; (B) lesions crossed by one/more vessels; (C) lesions in artifacts area. Lesions are magnified in a rectangle on the bottom right and indicated with a red arrow. QSM = quantitative susceptibility mapping. [Color figure can be viewed at www.annalsofneurology.org]

lesions where the majority of the volume was covered by a hyperintense vessel), (2) susceptibility artifacts (19.96%), and (3) confluency (4.42%; Fig 3).

Mean Susceptibility in all WMLs. We averaged quantitative susceptibility, MWF, and NDI values in WM of HCs and in NAWM of patients with MS. There was no significant difference in age between patients with MS and HCs ($p > 0.05$). The patient-wise average of magnetic susceptibility in WMLs in patients with MS ($n = 104$) was not different from the susceptibility in NAWM nor from the

WM in HCs (WM-HCs; $p > 0.05$). However, the average susceptibility was lower in NAWM than in WM-HCs ($p = 0.014$; Fig 4A).

Lesion-wise analysis of 2,852 WMLs showed that the susceptibility in MS WMLs relative to PPWM exhibited values ranging from -163.7 ppb to $+159.00$ ppb (5.04 [0.99–13.52], median [interquartile range]). Moreover, 814 of 2,852 WMLs (28.54%) exhibited a negative relative susceptibility and 2,038 of 2,852 WMLs (71.46%) had a positive relative susceptibility (see Fig 4B).

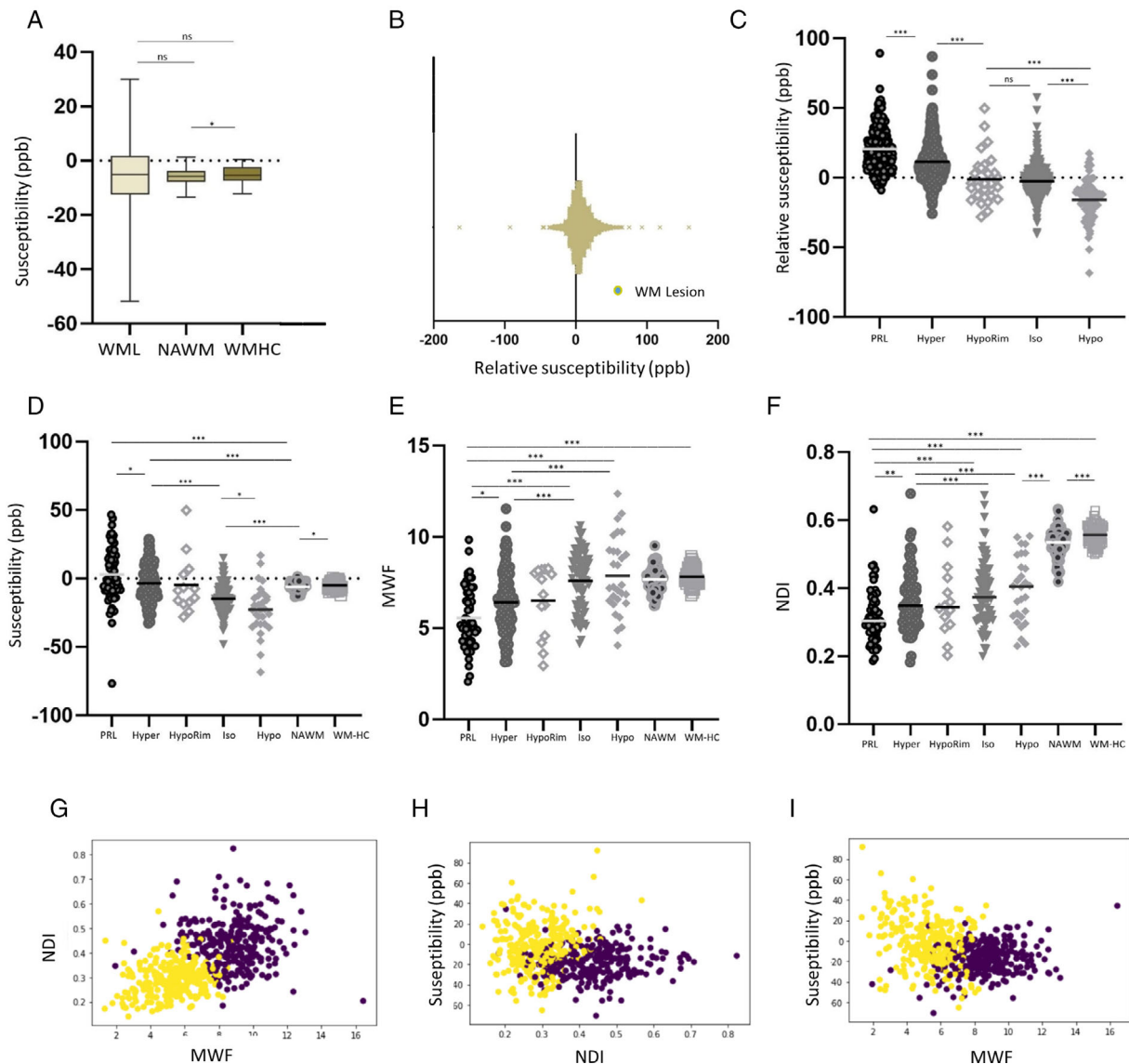


Figure 4: Quantitative susceptibility, MWF, and NDI in QSM lesion types. (A) Average susceptibility in WMLs, NAWM, and WM-HCs. (B) Lesion-wise relative susceptibility of WMLs compared to PPWM. (C) Comparison of mean relative susceptibility values among QSM lesion types. (D–F) Comparison of susceptibility, MWF, and NDI values among QSM lesion types. (G–I) GMM clustering of WMLs using mean lesion MWF, NDI, and susceptibility. * $p < 0.05$; ** $p < 0.001$; *** $p < 0.0001$. GMM = Gaussian Mixture Model; MWF = myelin water fraction; NAWM = normal-appearing white matter; NDI = neurite density index; ppb = parts per billion; PPWM = peri-plaque white matter; QSM = quantitative susceptibility mapping; WM = white matter; WM-HCs = white matter healthy controls; WML = white matter lesions. [Color figure can be viewed at www.annalsofneurology.org]

As to the relationship between susceptibility measures and disease duration, we found a significant correlation between absolute/relative susceptibility in WMLs and disease duration ($r = -0.32$ and $p = 0.0009$ and $r = -0.19$ & $p < 0.0001$, respectively), but not for absolute/relative susceptibility in NAWM and disease duration ($r = -0.09066$ and $p = 0.37$).

Mean Susceptibility Comparison across QSM Lesion Types

The comparison of the relative susceptibility across groups revealed that hypo-intense lesions have lower relative magnetic susceptibility than iso-intense lesions ($p < 0.0001$), iso-intense lesions exhibit lower relative magnetic susceptibility than hyperintense lesions ($p < 0.0001$), and hyperintense lesions show lower relative magnetic susceptibility than PRLs ($p < 0.0001$; see Fig 4C).

Further, hypo-intense lesions in QSM images show lower absolute magnetic susceptibility than iso-intense lesions ($p = 0.0081$), iso-intense lesions show lower absolute magnetic susceptibility than hyperintense lesions ($p < 0.0001$), and hyperintense lesions show lower absolute magnetic susceptibility than PRLs ($p = 0.014$; see Fig 4D).

Comparison of Mean Susceptibility between Lesions with Predominant Axon or Myelin Loss

WMLs ($n = 85$) exhibiting contralateral mirror areas without focal lesions were selected and categorized into lesions with dominant axon or myelin damage according to the relative MWF and NDI changes. However, there was no difference in the average susceptibility between lesions with predominant axon or myelin damage (4.06 ± 17.67, 7.76 ± 21.80, respectively; $p > 0.05$). In addition, no difference was found when the mean NDI was compared between lesions with positive and negative relative susceptibility (0.36 ± 0.11, 0.35 ± 0.11, respectively; $p > 0.05$).

MWF and NDI in QSM Lesion Types

Iso-intense lesions exhibited higher NDIs ($p < 0.05$) and MWFs ($p < 0.0001$) compared with QSM-visible lesions. Iso-intense lesions also exhibited lower NDIs compared with that of NAWM and WM-HCs (both $p < 0.0001$). On the other hand, the MWF of iso-intense lesions was not different from that of NAWM or WM-HCs (both $p > 0.05$). Nevertheless, iso-intense lesions exhibited higher MWFs and NDIs than hyperintense lesions and PRLs (both $p < 0.0001$; see Fig 3E, F). Last, there was no difference in MWFs and NDIs between iso-intense and hypo-rim lesions (both $p > 0.05$; see Fig 4E, F).

Hypo-intense lesions exhibited lower NDIs compared with that of NAWM and WM-HCs (both $p < 0.0001$). On the other hand, the MWF of hypo-intense lesions was not different from that of NAWM or WM-HCs (both $p > 0.05$). In comparison with other QSM lesion types, hypointense lesions showed higher MWFs and NDIs than did hyperintense lesions and PRLs (both $p < 0.0001$; see Fig 4E, F). The MWF was lower in hypo-rim lesions than in hypo-intense lesions ($p < 0.05$; see Fig 4E, F), however, the NDI did not differ ($p > 0.05$; see Fig 4E, F).

Hyperintense lesions exhibited lower MWFs and NDIs compared with that of NAWM and WM-HCs (both $p < 0.0001$), and higher MWFs and NDIs compared with that of PRLs ($p = 0.0029$ and $p < 0.001$; see Fig 4E, F, respectively). In addition, PRLs showed lower

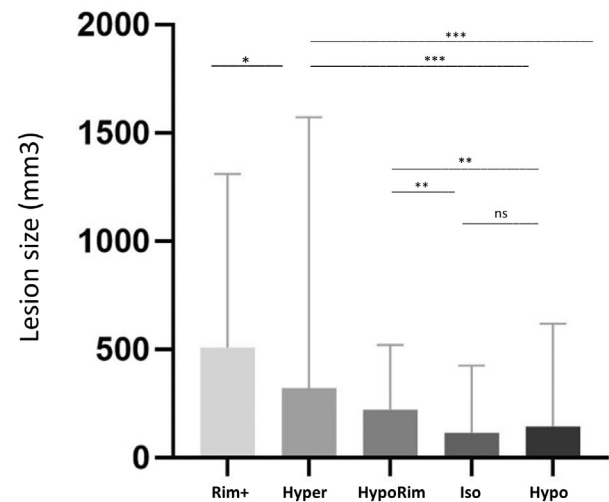


Figure 5: Lesion size comparison across QSM lesion types. * $p < 0.05$; ** $p < 0.001$; *** $p < 0.0001$. Iso = iso-intense; ns = not significant; QSM = quantitative susceptibility mapping.

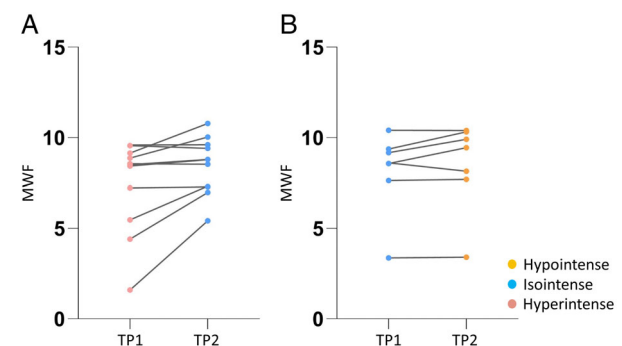


Figure 6: MWF changes in iso- and hypo-intense lesions at follow-up (TP2) compared to baseline (TP1). (A) MWF increases in the majority of lesions that are hyperintense at TP1 and iso-intense at TP2. (B) MWF is stable in lesions that are iso-intense at TP1 and hypo-intense at TP2. MWF = myelin water fraction; TP1 = timepoint1; TP2 = timepoint2. [Color figure can be viewed at www.annalsofneurology.org]

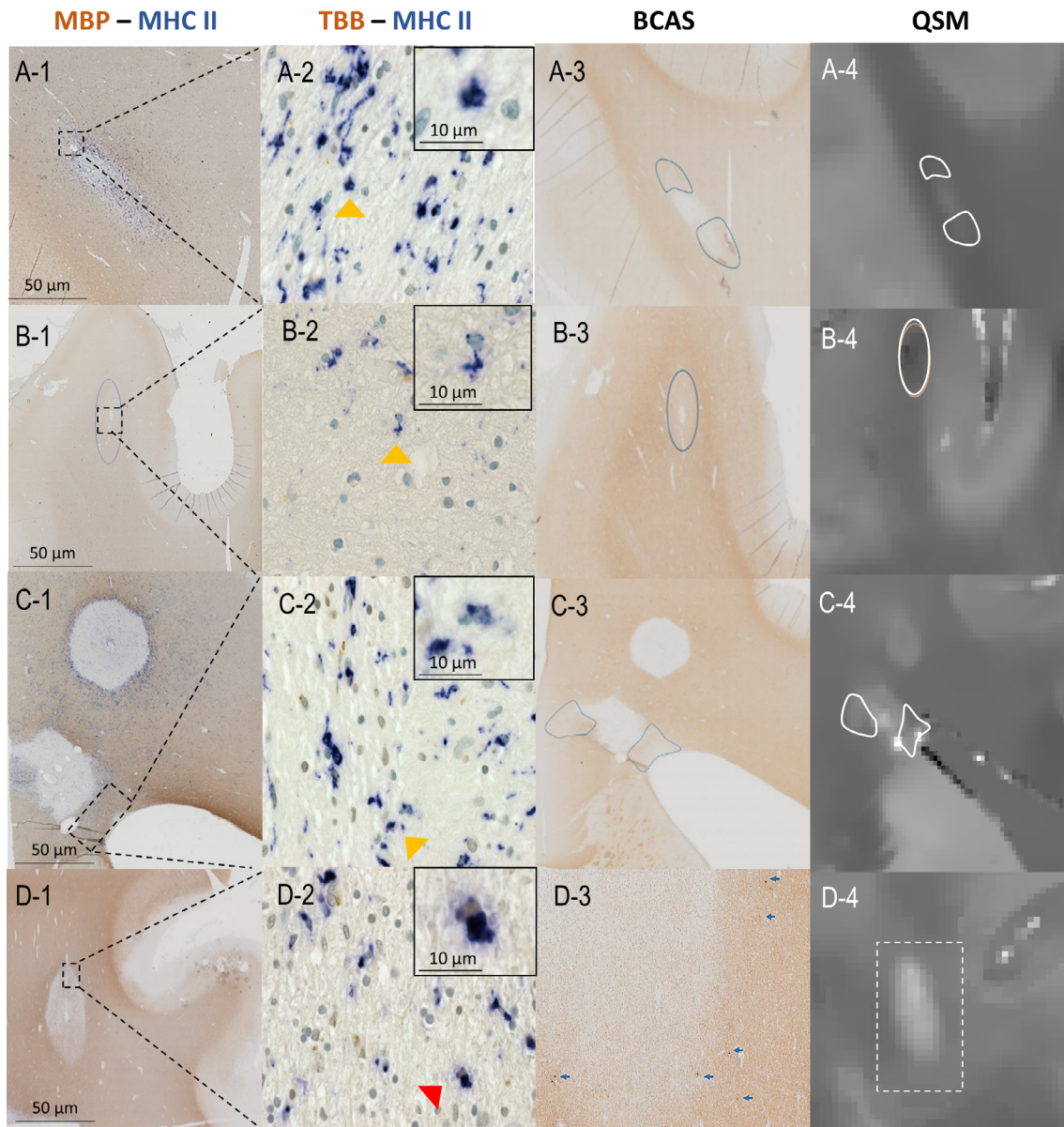


Figure 7: Histopathology and postmortem QSM of remyelinated lesions. A1–D1: MBP (brown)-MHC II (blue) double IHC in exemplary fully (B-1) or partially (A1, C1, D1) remyelinated lesions. **A2–D2:** DAB-enhanced TBB (brown) - MHC II (blue) staining showing macrophages/activated microglia containing (D1; red arrow) or lacking iron (A1–C1; yellow arrow); **A3–D3:** BCAS1 IHC showing non-compact myelin and, in D-3, newly formed myelinating oligodendrocytes; **A4–D4:** postmortem QSM showing fully (B-1) or partially (A1, C1, D1) remyelinated lesions. [Color figure can be viewed at www.annalsofneurology.org]

MWFs and NDIs compared with WM-HCs, NAWM, and all other QSM lesion types (all $p < 0.01$; see Fig 4E, F).

Comparison of Lesion Size Across QSM Lesion Types

Hypo-intense lesions and iso-intense lesions were smaller than hyperintense lesions (both $p < 0.0001$), which in turn were smaller than PRLs ($p < 0.05$; Fig 5).

Comparison of QSM Lesion Type Frequency between RRMS and PMS and between Different Anatomic Locations

There was no difference in the frequency of QSM lesion types between patients with RRMS and PMS (see Fig 1; all $p > 0.05$). PRLs were predominantly located in PV regions ($p < 0.05$) and hypo-intense lesions mainly in JC areas ($p < 0.001$). Iso-intense and hyperintense lesions were evenly distributed across PV, DW, and JC regions.

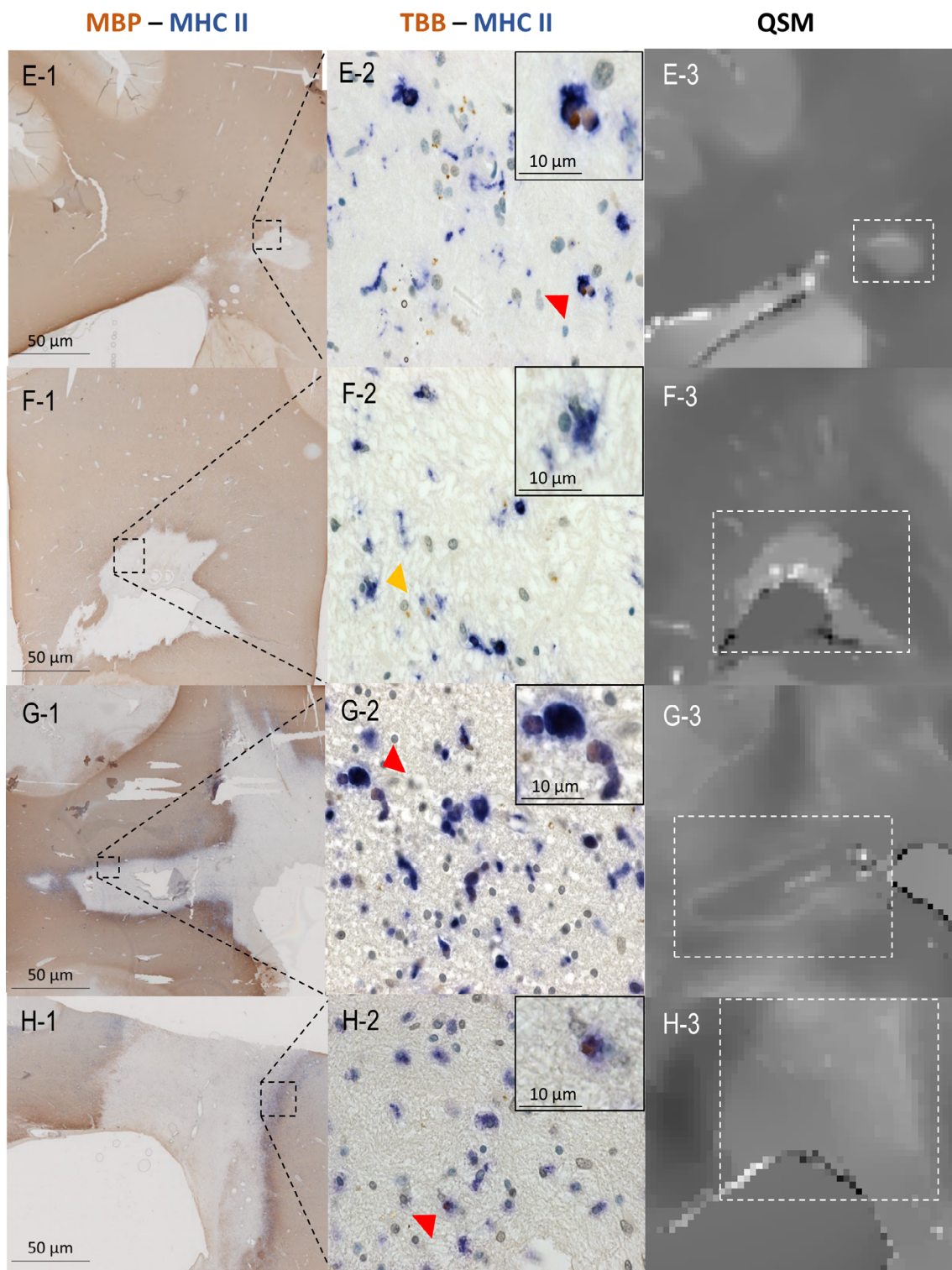


Figure 8: Histopathology and postmortem QSM of chronic inactive and chronic active lesions. **E1–F1:** MBP - MHC II staining of chronic inactive lesions. **E2–F2:** TBB (brown) - MHC II (blue) staining of macrophages/activated microglia containing (E2; red arrow) or lacking iron (F2; yellow arrow). **E-3, F-3:** Postmortem QSM showing a corresponding hyperintensity for chronic inactive lesions. **G1–H1:** MBP - MHC II IHC of chronic active lesions showing extensive demyelination. **G2–H2:** TBB (brown) - MHC II (blue) staining showing iron-laden macrophages/activated microglia at the lesion edge (red arrow). **G-3, H-3:** Postmortem QSM revealing a hyperintense paramagnetic rim in chronic active lesions. BCAS1 = breast carcinoma-amplified sequence 1; IHC = immunohistochemistry; MBP = myelin basic protein; MHC II = major histocompatibility complex II; QSM = quantitative susceptibility mapping; TBB = DAB-enhanced Turnbull's blue. [Color figure can be viewed at www.annalsofneurology.org]

Table 2. Sensitivity and Specificity of QSM Classification to Distinct Histopathological MS Lesion Types

Histopathological MS lesion types	QSM-lesion phenotype	QSM classification sensitivity	QSM classification specificity
Remyelinated	Iso-/hypo-intense	88.89%	100%
Chronic inactive	Hyperintense	71.43%	92.00%
Chronic active	Rim+ lesions	92.86%	86.36%

QSM = quantitative susceptibility mapping; MS = multiple sclerosis.

Longitudinal Evaluation of Iso- and Hypo-intense Lesions

To confirm our cross-sectional observations suggesting that iso- and hypo-intense lesions were remyelinated lesions, we performed a longitudinal study in 40 patients. Specifically, we assessed how MWF changed between baseline MRI and follow-up MRI in lesions that appear iso- and hypo-intense in QSM maps at follow-up.

Out of 325 WM lesions in follow-up QSM, 18 lesions were iso- and hypo-intense and had a corresponding lesion in baseline QSM images.

Of those, 8 of 18 hypo- and iso-intense lesions at follow-up were iso- or hypo-intense, respectively, at baseline. In these lesions, MWF remained overall stable over time (average increase of 3.61%, mean MWF baseline = 8.15, and TP2 follow-up = 8.47; Fig 6).

However, 10 of 18 hypo/iso-intense lesions at follow-up were hyperintense at baseline: those lesions showed an average increase of 33.55% in MWF (mean MWF baseline = 7.39 and follow-up = 8.45).

Clustering of Iso-/Hypo-intense Lesions vs PRLs

To confirm that the qualitative appearance of QSM lesion types represents lesions with different MWFs, NDIs, and susceptibility, a GMM was applied to the lesion groups exhibiting the highest and lowest MWF and NDI mean content.

When PRLs and hypo-intense/iso-intense lesions were considered, the GMM identified 2 clusters: 80.23% of PRLs clustered in the area with low MWF and NDI values (see yellow cluster in Fig 4G–I), whereas 72.55% of hypo-intense and 68.15% of iso-intense lesions clustered in the area with high MWF and NDI values (see purple cluster in Fig 4G–I).

Histopathology and QSM Study

To further investigate the relationship between QSM lesion types and histopathological lesion categories, we performed a histopathology-QSM study in 3 brains including 63 WM MS lesions.

Eight out of 9 (88.88%) remyelinated lesions/areas appeared iso- or hypo-intense in QSM maps. However, all lesions (8 out of 8–100%) detected as iso and hypo-intense in QSM were remyelinated lesions/areas (Fig 7A–D). The only remyelinated lesion not appearing iso- or hypo-intense was hyperintense (n = 1) in QSM images. This hyperintense remyelinated lesion was characterized by iron-rich macrophages/activated microglia and incomplete remyelination (see Fig 7D).

Ten out of 14 (71.43%) chronic inactive lesions/areas appeared hyperintense in QSM maps and the other 4 were PRLs (28.57%). Ten out of 14 QSM hyperintense lesions were chronic inactive lesions/area without signs of lesion activity (Fig 8E–H) and the remaining 4 were chronic active (n = 3) and remyelinated lesions (n = 1) with iron-laden macrophages/microglia.

Thirty-seven out of 40 (92.5%) chronic active lesions/areas appeared as PRL in QSM maps and the remaining 3 as hyperintense lesions (7.5%). On the other hand, 39 out of 42 (92.85%) QSM PRLs appeared as chronic active lesions/areas with iron-laden macrophages/microglia at lesion border (Fig 8G, H) and the remaining 3 were chronic inactive (n = 3).

Table 2 summarizes the sensitivity and specificity of QSM classification to identify distinct neuropathological MS lesions types.

Discussion

In this work, we identified 5 QSM lesions types in vivo in patients with MS and quantified their relative axon and myelin content using myelin-water and diffusion imaging. These 5 QSM lesion types exhibited imaging features that were compatible with specific histopathological lesion subtypes, namely (1) remyelinated (iso- and hypo-intense lesions), (2) chronic inactive (hyperintense lesions), and (3) chronic active/smoldering lesions (PRLs). An additional combined postmortem QSM-histopathology study confirmed these associations.

Previous work related some characteristics of MS lesions on QSM maps to lesion age and to the presence of acute and chronic focal inflammation. Specifically, acute lesions were shown to exhibit susceptibility values that were very close to that of the surrounding NAWM,⁷ whereas chronic active/smoldering lesions were described as plaques with a paramagnetic rim, which corresponds to iron-rich macrophages and activated microglia (PRLs).^{6,7,47}

In this study, we identified several QSM lesion types that had been previously described (PRLs, hyperintense, and iso-intense lesions⁴⁸) and some other rarer types that we report here for the first time (hypo-intense and hyporim lesions). Furthermore, we present new evidence indicating that QSM lesion types differ substantially in their myelin and axon content, as measured by surrogate imaging measures, such as MWF and NDI.

In accordance with previous neuropathological⁴⁹ and imaging studies,⁵⁰ the majority of WMLs in this cohort of patients with MS showed a positive relative susceptibility on QSM maps (hyperintense lesions). This is probably driven by iron accumulation in microglia, macrophages, and oligodendrocytes⁵¹ (especially when the relative susceptibility is >60 ppb⁵²) and/or by loss of myelin integrity.^{3,52–54}

Interestingly, the range of relative magnetic susceptibility within each QSM lesion subtype was found to be quite broad suggesting that the pathological features within each lesion group are part of a spectrum and/or that the surrounding NAWM is variably affected in different patients.

Magnetic susceptibility across QSM lesion subtypes was also inversely related to the MWF and NDI (see Fig 2D–I). Lesions with the highest relative susceptibility (ie, PRLs and hyperintense lesions) also showed the lowest MWFs and NDIs, suggesting that iron deposition in those lesions lead to pro-inflammatory microglia-activation and to amplification of neurodegeneration.^{5,55,56}

Our results show that although most of the WMLs in patients with MS exhibit higher susceptibility compared with the one measured in the immediate PP tissue (ie, positive relative susceptibility), both absolute and relative susceptibility decrease in the course of the disease. These results further confirm previous findings reporting a decrease in relative susceptibility in chronic MS lesions in comparison with other “moderately aged” lesions,⁷ and point either to a relative accumulation of iron in NAWM⁵⁷ or to a progressive loss of iron-rich cells (eg, activated microglia and oligodendrocytes) in WML.^{57–59}

PRLs have been previously described as QSM lesions characterized by a rim of activated and iron-rich microglia with accompanying smoldering demyelination and axonal

loss.^{4,6} Both our in vivo and postmortem results confirmed that these plaques are characterized by extensive myelin and axon damage and provided additional evidence that PRLs correspond to chronic active/smoldering lesions with high sensitivity and specificity (Table 2).^{3,4,6,47,60}

Our data also showed that hyperintense QSM lesions have high susceptibility and low mean MWFs and NDIs, suggesting extensive myelin/axon damage.⁴⁹ This was confirmed by our histopathological-MRI study, which revealed that QSM hyperintense lesions mostly correspond to chronic inactive plaques with extensive demyelination. Interestingly, a minority of histopathologically defined chronic inactive lesions (3/14) exhibited a paramagnetic rim in postmortem QSM, which did not correspond to iron accumulation within microglia/macrophages but, rather, to pronounced demyelination at the lesion edge. Last, consistent with previous QSM studies performed in vivo^{7,49,61} and work focusing on chronic inactive lesions postmortem,⁸ QSM hyperintense lesions were found to be the most frequent QSM lesion type in our cohort of patients.

Additionally, we identified a new QSM lesion type, hypointense QSM lesions, which showed the lowest susceptibility and the highest myelin and axon content compared with other QSM lesion types, suggesting that they may represent remyelinated plaques. The average MWF in these lesions was at the level of that measured in NAWM and in the WM of HCs. Moreover, it was higher than that of other QSM lesion types, including PRLs, hyporim, and hyperintense lesions. In line with this, fully remyelinated lesions with scarce macrophages/activated microglia and no signs of actively remyelinating oligodendrocytes⁶² appeared hypointense in postmortem QSM.

It remains unclear why an MS lesion appears hypointense in QSM images. It may be due to the different diamagnetic properties of the remyelinated axons showing thinner myelin and shorter internodal lengths^{63,64} and/or to their relatively low iron content compared with the peri-plaque region.⁶⁵ Supporting the latter explanation is the fact that hypo-intense lesions are predominant in the juxtacortical area, which is a region particularly rich in iron.⁶⁵ Thus, if myelin, but not iron, is restored in the lesion, remyelinated areas in this region may appear hypointense. Future studies focusing on this QSM lesion subtype may help to define the mechanisms driving this susceptibility change in QSM maps.

Iso-intense lesions have myelin content similar to that of hypo-intense lesions and higher than that of other QSM lesion types. However, iso-intense lesions exhibit higher susceptibility compared to that of hypo-intense lesions, probably due to higher iron content or incomplete remyelination, as evidenced postmortem. Given that acute

lesions show susceptibility that is very close to that of PPWM,⁷ Gd-enhancing lesions detected within a 3-month window of this study were excluded to avoid the inclusion of acute lesions in the isointense QSM lesion group.

Iso- and hypo-intense lesions exhibited 100% specificity to histopathologically defined remyelinated lesions. However, one remyelinated lesion appeared rather hyperintense leading to a sensitivity of 89%, probably due to the presence of iron-laden macrophages/microglia and incomplete remyelination. Hence, it appears that iso- and hypo-intensity in QSM indicates complete focal remyelination with no active microglia or macrophages. This interpretation is not only strongly suggested by our postmortem results, but was also confirmed by the fact that baseline hyperintense lesions that converted to iso- and hypo-intense lesions at follow-up exhibited an average 33.55% increase in MWF.

Further supporting the fact that hypo-intense and iso-intense lesions are most probably fully remyelinated plaques is the observation of significantly less axon damage in these lesions compared with other lesions (as measured by NDI), as it was reported in previous neuropathological studies.^{66,67}

Last, MS lesions rarely appear with a hypo-intense rim around a relatively hyperintense center in QSM. We hypothesize that lower susceptibility at the edge of the lesions compared with the center could signify destructive damage leading to tissue loss, probably in late stages of chronic active/smoldering lesions. Unfortunately, none of these lesions were identified in the 2 brains evaluated post-mortem, which could be due to the rarity of this lesion type. Therefore, further studies will be needed to fully test this hypothesis.

It should be noted that although excessive iron accumulation may put demyelinated axons under devastating oxidative stress,^{15,51} our data showed that axonal damage did not differ between lesions with positive relative susceptibility and lesions with negative relative susceptibility. Further, susceptibility was not different between lesions with predominant-axonal damage and those with predominant-myelin damage. The contribution of both iron and myelin content to QSM susceptibility⁵³ as well as the dual role of iron in oxidative damage^{15,51} and in fostering remyelination and repair⁶⁸ may partly account for these findings.

Interestingly, PRLs were mainly located around the ventricles, a region characterized by destructive plaques, possibly owing to the release of immune cells and cytokines from the ventricles.^{69,70} In contrast, hypo-intense lesions were mainly located in the juxta-cortical area, which is a region with potentially high remyelinating

capacity because of the presence of numerous oligodendrocyte precursor cells.^{10,71} Surprisingly, however, the distribution of QSM lesion types did not differ between patients with RRMS and PMS in our cohort. This shows once more that differences in MS lesion types are not associated with different clinical phenotypes.⁷² It is currently not clear whether RRMS and PMS are different pathological entities or different presentations of the same disease. Previously, we have shown that distribution of axon and myelin pathology in both focal lesions and in NAWM is similar between RRMS and PMS,⁴² a finding that is in line with neuropathological studies showing that WMLs in PMS and RRMS are qualitatively similar.^{58,72} Our current data showing that there was no significant difference in the frequency of QSM lesion types between patients with RRMS and PMS further corroborate the similarities in focal pathology between patients with RRMS and PMS.

One limitation of the current study is that a contrast-agent was not used for the identification of acute lesions at the time of MRI, therefore, some of the iso-intense lesions might have been acute lesions; however, a conventional MRI with gadolinium injection was performed within 3 months of the advanced MRI performed in this study, which allowed a reasonable exclusion of acute lesions from the classification. Another limitation of this work is that a histopathological correlate of hypo-intense rim lesions could not be identified due to their rarity. Future studies including a larger number of autoptic evaluations should clarify the nature of this type of lesion. Further, a limited number of brains from patients with progressive MS were used for imaging-histopathology analyses. This, together with the fact that those patients were in their middle-elderly years, might well have influenced the extent of focal remyelination processes that were identified.

In addition, we excluded several MS lesions from the current classification because they were either traversed by multiple vessels or confluent, or affected by streaking artifacts. Future work should therefore aim to further refine the reconstruction of QSM maps to minimize the impact of artifactual areas in the lesion classification on QSM maps; besides, multiparametric studies should be planned to assess the combined information of QSM maps and other microstructural brain maps, such as quantitative T1, for a more comprehensive classification of lesion heterogeneity in MS.⁷³

To date, numerous treatments are available that target the acute inflammatory component of MS; however, drugs fostering remyelination and repair are lacking. The identification of imaging biomarkers of axonal and myelin repair is fundamental to drive the development of targeted

neuroprotective and reparative drugs. This work provides new evidence that QSM maps may be used to identify fully remyelinated lesions *in vivo* in patients with MS, providing a perspective to evaluate, at least in part, the repair capacity of existing and novel MS therapies using a single scan.

As to the potential application of this classification in clinical practice: susceptibility-based acquisition methods are feasible in clinical practice and data suitable for QSM evaluations may be acquired with both gradient-echo (GRE) type or EPI type of sequences. Nevertheless, further work is still required to integrate available QSM reconstruction algorithms into the clinical neuroradiological workflow.

In summary, our findings show that QSM maps permit the classification of MS lesions with various extents of damage and repair to myelin and axons. In addition, our multiparametric cross-sectional and longitudinal data, together with our double-blinded postmortem analyses, showed that QSM provides highly sensitive and specific biomarkers of completed remyelination.

Acknowledgments

Reza Rahmzadeh is supported by the MSIF-ECTRIMS McDonald fellowship, Multiple Sclerosis International Federation (MSIF-ECTRIMS.2019) and the Swiss Government Excellence Scholarship (Nr.2019.0539). Cristina Granziera is funded by the Swiss National Science Foundation (SNSF) grant PP00P3_176984, the Stiftung zur Förderung der gastroenterologischen und allgemeinen klinischen Forschung, EUROSTAR E!113682 HORIZON2020. Francesco La Rosa is supported by the European Union's Horizon 2020 research and innovation program under the Marie Skłodowska-Curie project TRABIT (agreement # 765148). Martina Absinta is supported by the Conrad N. Hilton foundation (grant # 17313). Daniel S. Reich, Pascal Sati, and Martina Absinta are partially funded by the Intramural Research Program of the National Institute of Neurological Disorders and Stroke, National Institutes of Health, USA. Matthias Weigel is paid by the Swiss National Science Foundation (SNSF) grant PP00P3_176984 and he has also received research funding by Biogen for developing spinal cord MRI. Open access funding provided by Universität Basel.

Author Contributions

R.R. and C.G. contributed to the conception and design of the study. R.R., R.G., E.B., P.J.L., M.B., M.W., J.F., T.D.N., P.S., S.S., A.D., F.L.R., M.A., P.S., M.B.C., E.-W.R., D.L., C.S., W.B., L.K., J.K., D.S.R., Y.W., and

C.G. contributed to the acquisition and analysis of data. R.R. and C.G. contributed to drafting the text and preparing the figures.

Potential Conflicts of Interests

Nothing to report.

References

1. Wang Y, Spincemille P, Liu Z, et al. Clinical quantitative susceptibility mapping (QSM): biometal imaging and its emerging roles in patient care. *J Magn Reson Imaging* 2017;46:951–971. <https://doi.org/10.1002/jmri.25693>.
2. Granziera C, Wuerfel J, Barkhof F, et al. Quantitative magnetic resonance imaging towards clinical application in multiple sclerosis. *Brain* 2021;144:1296–1311. <https://doi.org/10.1093/brain/awab029>.
3. Bagnato F, Hametner S, Yao B, et al. Tracking iron in multiple sclerosis: a combined imaging and histopathological study at 7 tesla. *Brain* 2011;134:3602–3615. <https://doi.org/10.1093/brain/awr278>.
4. Dal-Bianco A, Grabner G, Kronnerwetter C, et al. Slow expansion of multiple sclerosis iron rim lesions: pathology and 7 T magnetic resonance imaging. *Acta Neuropathol* 2017;133:25–42. <https://doi.org/10.1007/s00401-016-1636-z>.
5. Stephenson E, Nathoo N, Mahjoub Y, et al. Iron in multiple sclerosis: roles in neurodegeneration and repair. *Nat Rev Neurol* 2014;10:459–468. <https://doi.org/10.1038/nrneurol.2014.118>.
6. Absinta M, Sati P, Schindler M, et al. Persistent 7-tesla phase rim predicts poor outcome in new multiple sclerosis patient lesions. *J Clin Invest* 2016;126:2597–2609. <https://doi.org/10.1172/Jci86198>.
7. Chen W, Gauthier SA, Gupta A, et al. Quantitative susceptibility mapping of multiple sclerosis lesions at various ages. *Radiology* 2014;271:183–192. <https://doi.org/10.1148/radiol.13130353>.
8. Lassmann H. Multiple sclerosis pathology. *Cold Spring Harb Perspect Med* 2018;8:a028936. <https://doi.org/10.1101/cshperspect.a028936>.
9. Kuhlmann T, Ludwin S, Prat A, et al. An updated histological classification system for multiple sclerosis lesions. *Acta Neuropathol* 2017;133:13–24. <https://doi.org/10.1007/s00401-016-1653-y>.
10. Patrikios P, Stadelmann C, Kutzelnigg A, et al. Remyelination is extensive in a subset of multiple sclerosis patients. *Brain* 2006;129:3165–3172. <https://doi.org/10.1093/brain/awl217>.
11. Goldschmidt T, Antel J, König FB, et al. Remyelination capacity of the MS brain decreases with disease chronicity. *Neurology* 2009;72:1914–1921. <https://doi.org/10.1212/WNL.0b013e3181a8260a>.
12. Kuhlmann T, Miron V, Cui Q, et al. Differentiation block of oligodendroglial progenitor cells as a cause for remyelination failure in chronic multiple sclerosis. *Brain* 2008;131:1749–1758. <https://doi.org/10.1093/brain/awn096>.
13. Lassmann H, van Horssen J, Mahad D. Progressive multiple sclerosis: pathology and pathogenesis. *Nat Rev Neurol* 2012;8:647–656. <https://doi.org/10.1038/nrneurol.2012.168>.
14. Kuhlmann T, Lingfeld G, Bitsch A, et al. Acute axonal damage in multiple sclerosis is most extensive in early disease stages and decreases over time. *Brain* 2002;125:2202–2212. <https://doi.org/10.1093/brain/awf235>.
15. Friese MA, Schattling B, Fugger L. Mechanisms of neurodegeneration and axonal dysfunction in multiple sclerosis. *Nat Rev Neurol* 2014;10:225–238. <https://doi.org/10.1038/nrneurol.2014.37>.

16. Tham M, Frischer JM, Weigand SD, et al. Iron heterogeneity in early active multiple sclerosis lesions. *Ann Neurol* 2020;89(3):498–510. <https://doi.org/10.1002/ana.25974>.
17. Popescu BF, Frischer JM, Webb SM, et al. Pathogenic implications of distinct patterns of iron and zinc in chronic MS lesions. *Acta Neuropathol* 2017;134:45–64. <https://doi.org/10.1007/s00401-017-1696-8>.
18. Laule C, Moore GRW. Myelin water imaging to detect demyelination and remyelination and its validation in pathology. *Brain Pathol* 2018;28:750–764. <https://doi.org/10.1111/bpa.12645>.
19. Nguyen TD, Deh K, Monohan E, et al. Feasibility and reproducibility of whole brain myelin water mapping in 4 minutes using fast acquisition with spiral trajectory and adiabatic T2prep (FAST-T2) at 3T. *Magn Reson Med* 2016;76:456–465. <https://doi.org/10.1002/mrm.25877>.
20. Cercignani M, Gandini W-KC. From micro- to macro-structures in multiple sclerosis: what is the added value of diffusion imaging. *NMR Biomed* 2019;32:e3888. <https://doi.org/10.1002/nbm.3888>.
21. Moore GR, Leung E, MacKay AL, et al. A pathology-MRI study of the short-T2 component in formalin-fixed multiple sclerosis brain. *Neurology* 2000;55:1506–1510. <https://doi.org/10.1212/wnl.55.10.1506>.
22. Kozłowski P, Rosicka P, Liu J, et al. In vivo longitudinal myelin water imaging in rat spinal cord following dorsal column transection injury. *Magn Reson Imaging* 2014;32:250–258. <https://doi.org/10.1016/j.mri.2013.12.006>.
23. Kaden E, Kelm ND, Carson RP, et al. Multi-compartment microscopic diffusion imaging. *Neuroimage* 2016;139:346–359. <https://doi.org/10.1016/j.neuroimage.2016.06.002>.
24. Bagnato F, Franco G, Thomas N, et al. Multi-compartment spherical microscopic diffusion imaging using spherical mean techniques to probe axonal injury in multiple sclerosis. *Neurology* 2018;90:P3.383.
25. Grussu F, Schneider T, Tur C, et al. Neurite dispersion: a new marker of multiple sclerosis spinal cord pathology? *Ann Clin Transl Neurol* 2017;4:663–679. <https://doi.org/10.1002/acn3.445>.
26. Colgan N, Siow B, O'Callaghan JM, et al. Application of neurite orientation dispersion and density imaging (NODDI) to a tau pathology model of Alzheimer's disease. *Neuroimage* 2016;125:739–744. <https://doi.org/10.1016/j.neuroimage.2015.10.043>.
27. Thompson AJ, Banwell BL, Barkhof F, et al. Diagnosis of multiple sclerosis: 2017 revisions of the McDonald criteria. *Lancet Neurol* 2018;17:162–173. [https://doi.org/10.1016/S1474-4422\(17\)30470-2](https://doi.org/10.1016/S1474-4422(17)30470-2).
28. Lublin FD, Reingold SC, Cohen JA, et al. Defining the clinical course of multiple sclerosis: the 2013 revisions. *Neurology* 2014;83:278–286. <https://doi.org/10.1212/WNL.0000000000000560>.
29. Nguyen TD, Wisnieff C, Cooper MA, et al. T2 prep three-dimensional spiral imaging with efficient whole brain coverage for myelin water quantification at 1.5 tesla. *Magn Reson Med* 2012;67:614–621. <https://doi.org/10.1002/mrm.24128>.
30. Jenista ER, Rehwald WG, Chen EL, et al. Motion and flow insensitive adiabatic T2 -preparation module for cardiac MR imaging at 3 tesla. *Magn Reson Med* 2013;70:1360–1368. <https://doi.org/10.1002/mrm.24564>.
31. Kumar D, Nguyen TD, Gauthier SA, Raj A. Bayesian algorithm using spatial priors for multiexponential T(2) relaxometry from multiecho spin echo MRI. *Magn Reson Med* 2012;68:1536–1543. <https://doi.org/10.1002/mrm.24170>.
32. Laule C, Leung E, Lis DK, et al. Myelin water imaging in multiple sclerosis: quantitative correlations with histopathology. *Mult Scler* 2006;12:747–753. <https://doi.org/10.1177/1352458506070928>.
33. Wang G, El-Sharkawy AM, Edelstein WA, et al. Measuring T(2) and T(1), and imaging T(2) without spin echoes. *J Magn Reson* 2012;214:273–280. <https://doi.org/10.1016/j.jmr.2011.11.016>.
34. Birkel C, Birkel-Toeglhofer AM, Endmayr V, et al. The influence of brain iron on myelin water imaging. *Neuroimage* 2019;199:545–552. <https://doi.org/10.1016/j.neuroimage.2019.05.042>.
35. Andersson JLR, Sotiropoulos SN. An integrated approach to correction for off-resonance effects and subject movement in diffusion MR imaging. *Neuroimage* 2016;125:1063–1078. <https://doi.org/10.1016/j.neuroimage.2015.10.019>.
36. Liu T, Xu W, Spincemaille P, et al. Accuracy of the morphology enabled dipole inversion (MEDI) algorithm for quantitative susceptibility mapping in MRI. *IEEE Trans Med Imaging* 2012;31:816–824. <https://doi.org/10.1109/TMI.2011.2182523>.
37. Wicaksono KP, Fushimi Y, Nakajima S, et al. Two-minute quantitative susceptibility mapping from three-dimensional Echo-planar imaging: accuracy, reliability, and detection performance in patients with cerebral microbleeds. *Invest Radiol* 2021;56:69–77. <https://doi.org/10.1097/RLI.0000000000000708>.
38. Sun D, Yu Z, Fang X, et al. LncRNA GAS5 inhibits microglial M2 polarization and exacerbates demyelination. *EMBO Rep* 2017;18:1801–1816. <https://doi.org/10.15252/embr.201643668>.
39. La Rosa F, Abdulkadir A, Fartaria MJ, et al. Multiple sclerosis cortical and WM lesion segmentation at 3T MRI: a deep learning method based on FLAIR and MP2RAGE. *Neuroimage Clin* 2020;27:102335. <https://doi.org/10.1016/j.nicl.2020.102335>.
40. Jenkinson M, Beckmann CF, Behrens TE, et al. FSL. *Neuroimage* 2012;62:782–790. <https://doi.org/10.1016/j.neuroimage.2011.09.015>.
41. Gillen KM, Mubarak M, Park C, et al. QSM is an imaging biomarker for chronic glial activation in multiple sclerosis lesions. *Ann Clin Transl Neurol* 2021;8:877–886. <https://doi.org/10.1002/acn3.51338>.
42. Rahmanzadeh R, Lu PJ, Barakovic M, et al. Myelin and axon pathology in multiple sclerosis assessed by myelin water and multi-shell diffusion imaging. *Brain* 2021;144:1684–1696. <https://doi.org/10.1093/brain/awab088>.
43. Fischl B. FreeSurfer. *Neuroimage* 2012;62:774–781. <https://doi.org/10.1016/j.neuroimage.2012.01.021>.
44. Absinta M, Nair G, Filippi M, et al. Postmortem magnetic resonance imaging to guide the pathologic cut: individualized, 3-dimensionally printed cutting boxes for fixed brains. *J Neuropathol Exp Neurol* 2014;73:780–788. <https://doi.org/10.1097/NEN.0000000000000096>.
45. Yushkevich PA, Piven J, Hazlett HC, et al. User-guided 3D active contour segmentation of anatomical structures: significantly improved efficiency and reliability. *Neuroimage* 2006;31:1116–1128. <https://doi.org/10.1016/j.neuroimage.2006.01.015>.
46. Allan C, Burel JM, Moore J, et al. Omero: flexible, model-driven data management for experimental biology. *Nat Methods* 2012;9:245–253. <https://doi.org/10.1038/nmeth.1896>.
47. Hametner S, Wimmer I, Haider L, et al. Iron and neurodegeneration in the multiple sclerosis brain. *Ann Neurol* 2013;74:848–861. <https://doi.org/10.1002/ana.23974>.
48. Harrison DM, Li X, Liu H, et al. Lesion heterogeneity on high-field susceptibility MRI is associated with multiple sclerosis severity. *AJNR Am J Neuroradiol* 2016;37:1447–1453. <https://doi.org/10.3174/ajnr.A4726>.
49. Wisnieff C, Ramanan S, Olesik J, et al. Quantitative susceptibility mapping (QSM) of white matter multiple sclerosis lesions: interpreting positive susceptibility and the presence of iron. *Magn Reson Med* 2015;74:564–570. <https://doi.org/10.1002/mrm.25420>.
50. Bian W, Tranvinh E, Tournias T, et al. In vivo 7T MR quantitative susceptibility mapping reveals opposite susceptibility contrast between cortical and white matter lesions in multiple sclerosis. *AJNR Am J Neuroradiol* 2016;37:1808–1815. <https://doi.org/10.3174/ajnr.A4830>.
51. Ropele S, Enzinger C, Fazekas F. Iron mapping in multiple sclerosis. *Neuroimaging Clin N Am* 2017;27:335–342. <https://doi.org/10.1016/j.nic.2016.12.003>.

52. Li W, Wu B, Liu C. Quantitative susceptibility mapping of human brain reflects spatial variation in tissue composition. *Neuroimage* 2011;55:1645–1656. <https://doi.org/10.1016/j.neuroimage.2010.11.088>.
53. Deh K, Ponath GD, Molvi Z, et al. Magnetic susceptibility increases as diamagnetic molecules breakdown: myelin digestion during multiple sclerosis lesion formation contributes to increase on QSM. *J Magn Reson Imaging* 2018;48:1281–1287. <https://doi.org/10.1002/jmri.25997>.
54. Yao B, Bagnato F, Matsuura E, et al. Chronic multiple sclerosis lesions: characterization with high-field-strength MR imaging. *Radiology* 2012;262:206–215. <https://doi.org/10.1148/radiol.11110601>.
55. Adamczyk B, Adamczyk-Sowa M. New insights into the role of oxidative stress mechanisms in the pathophysiology and treatment of multiple sclerosis. *Oxid Med Cell Longev* 2016;2016:1973834. <https://doi.org/10.1155/2016/1973834>.
56. Haider L. Inflammation, iron, energy failure, and oxidative stress in the pathogenesis of multiple sclerosis. *Oxid Med Cell Longev* 2015;2015:725370. <https://doi.org/10.1155/2015/725370>.
57. Marik C, Felts PA, Bauer J, et al. Lesion genesis in a subset of patients with multiple sclerosis: a role for innate immunity? *Brain* 2007;130:2800–2815. <https://doi.org/10.1093/brain/awm236>.
58. Lucchinetti C, Bruck W, Parisi J, et al. Heterogeneity of multiple sclerosis lesions: implications for the pathogenesis of demyelination. *Ann Neurol* 2000;47:707–717. [https://doi.org/10.1002/1531-8249\(200006\)47:6<707::aid-ana3>3.0.co;2-q](https://doi.org/10.1002/1531-8249(200006)47:6<707::aid-ana3>3.0.co;2-q).
59. Lucchinetti C, Bruck W, Parisi J, et al. A quantitative analysis of oligodendrocytes in multiple sclerosis lesions. A study of 113 cases. *Brain* 1999;122:2279–2295. <https://doi.org/10.1093/brain/122.12.2279>.
60. Kaunzner UW, Kang Y, Zhang S, et al. Quantitative susceptibility mapping identifies inflammation in a subset of chronic multiple sclerosis lesions. *Brain* 2019;142:133–145. <https://doi.org/10.1093/brain/awy296>.
61. Li X, Harrison DM, Liu H, et al. Magnetic susceptibility contrast variations in multiple sclerosis lesions. *J Magn Reson Imaging* 2016;43:463–473. <https://doi.org/10.1002/jmri.24976>.
62. Todorich B, Pasquini JM, Garcia CI, et al. Oligodendrocytes and myelination: the role of iron. *Glia* 2009;57:467–478. <https://doi.org/10.1002/glia.20784>.
63. Lubetzki C, Zalc B, Williams A, et al. Remyelination in multiple sclerosis: from basic science to clinical translation. *Lancet Neurol* 2020;19:678–688. [https://doi.org/10.1016/S1474-4422\(20\)30140-X](https://doi.org/10.1016/S1474-4422(20)30140-X).
64. Lee J, Nam Y, Choi JY, et al. Mechanisms of T2 * anisotropy and gradient echo myelin water imaging. *NMR Biomed* 2017;30(4). <https://doi.org/10.1002/nbm.3513>.
65. Kirilina E, Helbling S, Morawski M, et al. Superficial white matter imaging: contrast mechanisms and whole-brain in vivo mapping. *Sci Adv*. 2020;6:eaa9281. <https://doi.org/10.1126/sciadv.aaz9281>.
66. Schultz V, van der Meer F, Wrzos C, et al. Acutely damaged axons are remyelinated in multiple sclerosis and experimental models of demyelination. *Glia* 2017;65:1350–1360. <https://doi.org/10.1002/glia.23167>.
67. Kornek B, Storch MK, Weisert R, et al. Multiple sclerosis and chronic autoimmune encephalomyelitis: a comparative quantitative study of axonal injury in active, inactive, and remyelinated lesions. *Am J Pathol* 2000;157:267–276. [https://doi.org/10.1016/S0002-9440\(10\)64537-3](https://doi.org/10.1016/S0002-9440(10)64537-3).
68. Lee NJ, Ha SK, Sati P, et al. Potential role of iron in repair of inflammatory demyelinating lesions. *J Clin Invest* 2019;129:4365–4376. <https://doi.org/10.1172/JCI126809>.
69. Magliozzi R, Howell O, Vora A, et al. Meningeal B-cell follicles in secondary progressive multiple sclerosis associate with early onset of disease and severe cortical pathology. *Brain* 2007;130:1089–1104. <https://doi.org/10.1093/brain/awm038>.
70. Wings KM, Gilden DH, Bennett JL, et al. Analysis of multiple sclerosis cerebrospinal fluid reveals a continuum of clonally related antibody-secreting cells that are predominantly plasma blasts. *J Neuroimmunol* 2007;192:226–234. <https://doi.org/10.1016/j.jneuroim.2007.10.009>.
71. Patani R, Balaratnam M, Vora A, Reynolds R. Remyelination can be extensive in multiple sclerosis despite a long disease course. *Neuropathol Appl Neurobiol* 2007;33:277–287. <https://doi.org/10.1111/j.1365-2990.2007.00805.x>.
72. Antel J, Antel S, Caramanos Z, et al. Primary progressive multiple sclerosis: part of the MS disease spectrum or separate disease entity? *Acta Neuropathol* 2012;123:627–638. <https://doi.org/10.1007/s00401-012-0953-0>.
73. Kolb H, Absinta M, Beck ES, et al. 7T MRI differentiates Remyelinated from demyelinated multiple sclerosis lesions. *Ann Neurol* 2021;90:612–626. <https://doi.org/10.1002/ana.26194>.